Finger-Like Lysing Patterns of Blood Clots

Aleksander Zidanšek,* Aleš Blinc,‡ Gojmir Lahajnar,* Dušan Keber,‡ and Robert Blinc*
*J. Stefan Institute, University of Ljubljana, 61111 Ljubljana, Slovenia; and ‡Trnovo Hospital of Internal Medicine, University Medical Center of Ljubljana, 61000 Ljubljana, Slovenia

ABSTRACT One-dimensional modeling of fibrinolysis (Senf, 1979; Zidanšek and Blinc, 1991; Diamond and Anand, 1993) has accounted for the dissolution velocity, but the shape of the lysing patterns can be explained only by two- or three-dimensional models. Here we report on finger-like drug-induced blood clot dissolution patterns obtained by proton nuclear magnetic resonance imaging, which can be described by the enzyme transport-limited system of fibrinolytic chemical equations with diffusion and perfusion terms (Zidanšek and Blinc, 1991) in the reaction time approximation if the random character of gel porosity is taken into account. A two-dimensional calculation based on the Hele-Shaw random walk models (Kadanoff, 1985; Liang, 1986) leads to fractal lysing patterns as, indeed, is observed. The fractal dimension of the experimental lysing patterns changes from 1.2 at the beginning of the experiments to a maximum of ~1.3 in the middle and then decreases toward one when the clot is recanalized.

INTRODUCTION

Dissolving coronary thrombi by administering thrombolytic drugs has improved survival in patients with myocardial infarction (Stampfer et al., 1982; Yusuf et al., 1985; GISSI, 1987; ISIS-2, 1988; AIMS, 1990), yet thrombolytic therapy is not universally successful and the physical origin of the various dissolution patterns has not been explained yet. Magnetic resonance imaging (MRI) has shown that clot dissolution proceeds in a finger-like manner whenever plasminogen activator enters the clot by pressure-induced flow (Blinc et al., 1993, 1994). Even when recanalization of the previously occluded vessel segment is achieved, dissolution of the blood clot is virtually never complete and a remaining thrombus often is found attached to the arterial wall.

The observed finger-like lysing patterns are here described by the enzyme transport-limited system of fibrinolytic chemical equations, taking into account the random character of the clot porosity.

MATERIALS AND METHODS

MRI experiments

We used an in vitro experimental approach for lysing occlusive blood clots under a pressure gradient, thus simulating thrombolysis under conditions of laminar blood flow (Blinc et al., 1991, 1993). Retracted clots were formed by mixing freshly drawn human venous blood with thrombin and calcium (Blinc et al., 1993). Adhesion of the retracted clots to the tube was secured by a tixothropic low reactive type polyester (by Helios, Domžale, Slovenia), which we found not to inhibit fibrinolysis of [^{125}I]fibrinogen-labeled blood clots. Occlusive clots were exposed to plasma containing 400 units/ml urokinase (Ukidan, Serono, Germany). The resulting plasma flow through the porous clots with a diameter of 4 mm under an initial pressure gradient of 2 kPa/cm (6 kPa pressure difference along 3-cm-long clots) was 1.0 ± 0.3 μl/min. The permeability (Darcy constant) of the retracted clot was thus 1.1×10^{-14} m^2 if the viscosity of plasma was taken as 1.7×10^{-3} kg m^{-1} s^{-1} at room temperature. This is less than 1% of the published permeability of nonretracted whole blood clots (Carr and Hardin, 1987). Dissolution of the clots was observed by spin-echo MRI, which distinguishes between nondissolved clot areas and dissolved areas that are replaced by inflowing plasma. A typical sequence of dissolution patterns is presented in Fig. 1 showing clot lysis in a finger-like pattern with the dominant finger progressing through the middle part of the clot.

Fibrinolytic system

We propose to explain our experimental results in terms of enzyme transport-limited chemical reactions occurring in the gel network. We have extended the previously described two-dimensional random walk models (Kadanoff, 1985; Liang, 1986) by introducing a nonzero reaction time. This approach allows for a discrete representation of equations linking the transport and enzymatic properties of the fibrinolytic system, which have been described in detail elsewhere (Zidanšek and Blinc, 1991; Zidanšek et al., 1993).

A thrombus is described as a homogeneous cylinder that is separated by a sharp boundary from the blood. The clot G has the boundary $B = B_1 \cup B_2 \cup B_3$, where B_1 is the inflowing blood-clot boundary, B_2 is the outflowing blood-clot boundary, and B_3 is the clot-vessel boundary (Fig. 2 *a*).

Plasminogen (PLG) is activated by plasminogen activator (A) into the active protease plasmin (P) in a process that can be described by Michaelis-Menten kinetics as

$$\mathrm{A} + \mathrm{PLG} \underset{k_{-1}}{\overset{k_1}{\rightleftharpoons}} \mathrm{E\text{-}S} \xrightarrow{k_2} \mathrm{A} + \mathrm{P},$$

where E-S is the intermediate enzyme-substrate complex. Plasmin is inactivated by a specific inhibitor, α_2-antiplasmin. If the concentration of plasmin remains small compared with the concentration of α_2-antiplasmin, inactivation of plasmin proceeds by pseudo-first-order kinetics:

$$\mathrm{P} \xrightarrow{k_3} \mathrm{P\text{-}AP},$$

Received for publication 6 March 1995 and in final form 23 May 1995.

Address reprint requests to Dr. Aleksander Zidanšek, J. Stefan Institute, University of Ljubljana, Jamova 39, 61111 Ljubljana, Slovenia. Tel.: 386-61-1773900; Fax: 386-61-219385; E-mail: aleksander.zidansek@ijs.si.

0006-3495/95/09/803/07 $2.00

where P-AP denotes the inactive plasmin-antiplasmin complex.

The system of fibrinolytic chemical equations with diffusion and perfusion transport can be approximated as (Zidanšek and Blinc, 1991):

$$\frac{\partial c_a}{\partial t} = D_a\nabla^2 c_a - v_F\nabla c_a - k_1 c_a c_{plg} + (k_{-1} + k_2)c_{es}, \quad (1)$$

$$\frac{\partial c_{es}}{\partial t} = D_{es}\nabla^2 c_{es} - v_F\nabla c_{es} + k_1 c_a c_{plg} - (k_{-1} + k_2)c_{es}, \quad (2)$$

$$\frac{\partial c_{plg}}{\partial t} = D_{plg}\nabla^2 c_{plg} - v_F\nabla c_{plg} - k_1 c_a c_{plg} + k_{-1}c_{es}, \quad (3)$$

$$\frac{\partial c_p}{\partial t} = D_p\nabla^2 c_p - v_F\nabla c_p + k_2 c_{es} - k_3 c_p. \quad (4)$$

Here c_a is the concentration of a non-fibrin-specific plasminogen activator such as urokinase, c_p is the concentration of plasmin, c_{plg} is the concentration of plasminogen, c_{es} is the concentration of the enzyme-substrate complex activator-plasminogen, k_1, k_2, k_{-1}, and k_3 are the reaction constants, D_a, D_p, D_{plg}, and D_{es} are the corresponding diffusion constants, and v_F is the perfusion flow velocity.

Initially, there is no plasminogen activator inside the clot and the plasminogen concentrations outside and inside the clot are assumed to be equal. The initial activator concentration in plasma is c_{a0}, and initial plasminogen concentration in the clot is c_{plg0}. If diffusion is neglected with respect to the flow, the boundary conditions for the activator and plasmin at the boundary B_1 are given as

$$c_a(\mathbf{r}) = c_{a0}, \qquad \mathbf{r} \in B_1, \quad (5)$$

$$c_p(\mathbf{r}) = 0, \qquad \mathbf{r} \in B_1, \quad (6)$$

and the normal derivatives of all concentrations equal zero at boundaries B_2 and B_3.

The clot is dissolved when more then ~1/3 of the plasmin-susceptible peptide bonds in the fibrin network are cleaved (Weinstein and Doolittle, 1972). The fibrin bond concentration c_f is initially equal to c_{f0} inside the clot and zero outside the clot. During the lysis fibrin bonds are cleaved, and the concentration c_f decreases as

$$\frac{\partial c_f}{\partial t} = -k_4 c_p c_f, \quad (7)$$

where k_4 is the reaction constant for the clot degradation, and the clot is dissolved at a given position $\mathbf{r}$, when the plasmin-susceptible fibrin bond concentration $c_f(\mathbf{r})$ falls to 2/3 of the initial value c_{f0}.

The fibrinolytic system can be mathematically treated in various ways. Simple one-dimensional models (Senf, 1979; Zidanšek and Blinc, 1991) have been extended to describe very complex reaction dynamics (Diamond and Anand, 1993). Here we analyze a simple two-dimensional model in the reaction time approximation. In the case of perfusion of clots with lytic plasma, the sequence of fibrinolytic reactions can be characterized with a single reaction time t_R representing the time lag between the arrival of the plasminogen activator and the actual clot dissolution at a given point (Zidanšek and Blinc, 1991).

If diffusion transport is negligible compared with the flow, a sharp boundary between the plasminogen activator-invaded part of the clot and the rest of the clot can be defined. The clot is thus divided into two parts:

- The reaction region between the inflow blood-clot boundary B_1 and the plasminogen activator front boundary B_4 (Fig. 2 *a*), and
- The clot region without any fibrinolytic enzymes.

Here the activator front boundary B_4 is determined by the flow of plasma with enzymes into the clot since the beginning of fibrinolysis. The plasma flow depends only on the pressure gradient, and the flow velocity $\mathbf{v}_F$ inside the clot is given by Darcy's law:

$$\mathbf{v}_F = -\frac{k}{\eta}\nabla p. \quad (8)$$

Here k is the Darcy permeability and η is the viscosity.

The boundary B_4 at the beginning of fibrinolysis ($t = 0$) is the same as

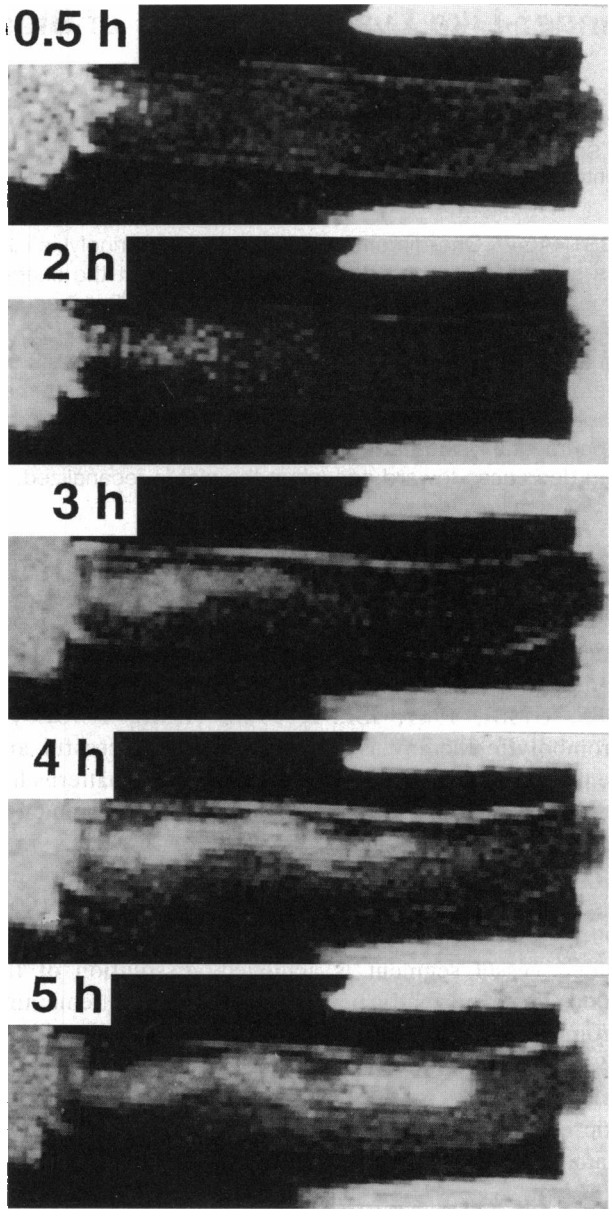

FIGURE 1 Magnetic resonance images of lysing patterns of a retracted blood clot exposed to pressure-induced perfusion with plasma-containing urokinase, obtained at 0.5, 2, 3, 4, and 5 h after the beginning of clot lysis. The fractal dimension of lysing patterns is between 1.3 and 1. MRI was performed in a 2.35 T-superconducting magnet with a spin-echo sequence. The recovery time was 2 s, the interecho time 60 ms, and the imaging time ~8.5 min with a 256 × 256 pixel matrix. Longitudinal views of clots were recorded with a 4-mm-slice thickness. Regions of interest from a 10-cm field of view are shown.

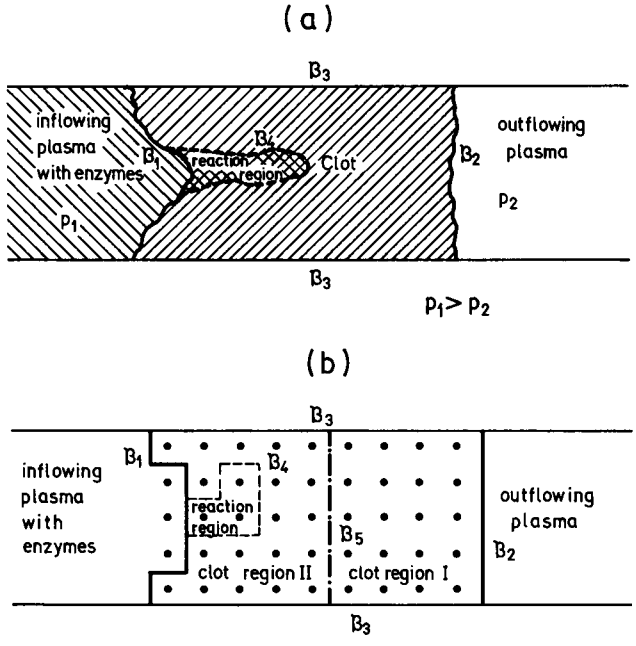

FIGURE 2 Schematic presentation of a blood clot and its boundaries. (*a*) In the reaction time approximation, the clot is divided into the reaction region and the region without the enzymes with the boundary B_4. B_1 is the inflowing blood-clot boundary, B_2 is the outflowing blood-clot boundary, and B_3 is the clot-vessel boundary. Here a sharp activator front boundary B_4 can be defined, if the enzyme diffusion is negligible in comparison with the flow transport. (*b*) Schematic presentation of the random walk model. Here the clot is represented as a two-dimensional network of points that are separated by the same boundaries as in *a*. The boundary B_5, which divides the clot into two regions, is added for the simplification of the random walk calculation.

B_1, because there are no enzymes inside the clot. A given position $\mathbf{r} \in B_4$ evolves with time as

$$\mathbf{r}(t) = \mathbf{r}(0) + \int_0^t \mathbf{v}_F(\mathbf{r}(t'))\, dt'. \tag{9}$$

The reaction at a given point $\mathbf{r}$ inside the reaction region starts when the activator front boundary reaches the point $\mathbf{r}$, and after the reaction time t_R the clot is dissolved at this point as shown by Zidanšek and Blinc, 1991. The time evolution of the inflow blood-clot boundary B_1 for times $t > t_R$ is thus given as

$$B_1(t) = B_4(t - t_R). \tag{10}$$

The fibrinolytic system of chemical reactions is now transformed into the problem of moving the boundaries B_1 and B_4 according to the above equations.

For the sake of mathematical convenience, we now go from a three- to a two-dimensional problem and replace the cylindrical geometry by a rectangular one (Fig. 2, *a* and *b*). At time $t = 0$ the clot is represented by a rectangle where the boundaries B_1 and B_4 are equal and represent the left (inflow) side of the rectangle, B_2 is the right (outflow) side, and the vessel-clot boundary B_3 is replaced by the long sides of the rectangle. The pressure p_1 at the inflow boundary B_1 is larger than the pressure p_2 at the outflow boundary B_2, and the normal component of the pressure gradient equals zero at the vessel-clot boundary B_3, because there is no flow through the vessel wall (Fig. 2, *a* and *b*). For a homogeneous medium, the analytical solution is the same as for the one-dimensional model (Zidanšek and Blinc, 1991): pressure is a linear function of the distance, the flow velocity is constant, and the lysing patterns are planar. We can also estimate the Reynolds number Re for the plasma flow through the clot as $\mathrm{Re} = vd/n\eta$, where v is the average velocity of the flow, d is the pore size, n is the porosity, and η is the viscosity. Typical values for the clot ($v \leq 10^{-4}$ m/s, $d \sim 10^{-6}$ m, $n \sim 0.1$, and $\eta \sim 1.7 \times 10^{-3}$ kg m^{-1} s^{-1}) yield $\mathrm{Re} \leq 10^{-6}$. Inclusion of the Brinkman correction (Martys et al., 1994) to Eq. 8 and the no-slip condition at the wall could also lead in principle to nonplanar lysis in the two-dimensional model with homogeneous media. The Brinkman equation can be written as

$$\nabla p = -\frac{\eta}{k}\mathbf{v}_F + \eta_e \nabla^2 \mathbf{v}_F, \tag{11}$$

where dynamic viscosity η_e is calculated to be of the same order of magnitude as viscosity η (Martys et al., 1994). Analytical solution of Brinkman's equation for a homogeneous medium in two dimensions is decreasing exponentially at the glass-clot boundary with a characteristic magnitude $y_0 = (k\eta_e/\eta)^{1/2} \sim 10^{-7}$ m. This is much too small to account for the observed effects. Flow velocity $\mathbf{v}_F$ is zero at the wall and reduced only at the distance a few y_0 from the wall. In the experimental case of a three-dimensional cylindrical clot $\mathbf{v}_F$ is also reduced only at the distance of the order y_0 from the glass-clot boundary and, thus, this correction seems not to be responsible for the nonplanar lysing patterns.

However, the analytical solution is unstable in the case of a nonhomogeneous clot structure or roughness in the boundary that is never exactly planar in real clots. Both possibilities are taken into account in the random walk type "pedestrian model" (Kadanoff, 1985). This model with zero surface tension is the same as the above described fibrinolytic model, if the reaction time $t_R = 0$ and, thus, $B_1 = B_4$. If $t_R > 0$, the "pedestrian model" (Liang, 1986) requires a modification (see Appendix A) because the boundary condition is given at the inflow boundary B_1 and the flow is observed at the activator front boundary B_4.

RESULTS AND DISCUSSION

A modified random walk calculation (Appendix A) was performed for different values of the reaction time t_R. If the nonzero reaction time t_R is taken into account, the dissolution patterns become wider and the dissolution is slower than in the zero reaction time model (Fig. 3). Here $t_R = (k_{-1} + k_2)k_3 \log 1.5/(k_1 k_2 k_4 c_{plg} c_{a0})$ (Zidanšek and Blinc, 1991), which is ~15 min, and the value $t_R = 500 t_0$ was used in our simulation (Fig. 3 *a*), where t_0 is the time of one lattice random walk between the two neighboring points. The time difference between the two patterns in Fig. 3 *a* is chosen as $\Delta t = 4t_R$, the lattice unit length $a \sim 0.2$ mm, the lattice width $W = 22$ lattice units, the lattice length $L = 100$ lattice units, and the time of one lattice random walk $t_0 \sim 2$ s.

The solutions of the random walk model of the clot dissolution depend on the magnitude of the dissolution time t_R: High values of t_R ($t_R \gg t_0$) are associated with finger-like patterns of clot dissolution (Fig. 3*a*, $t_R = 500\ t_0$), such as have been observed by MRI, and which are expected in arterial clots.

For very small values of t_R ($t_R \to 0$), diffusion-limited aggregation (DLA) patterns occur (Fig. 3 *b*) such as have been described in chemical dissolution of porous inorganic materials by an inflowing reactive fluid (Daccord and Lenormand, 1987).

One can calculate the fractal dimension of the fibrinolytic patterns, fitting the measured length $L(\delta)$ at different length

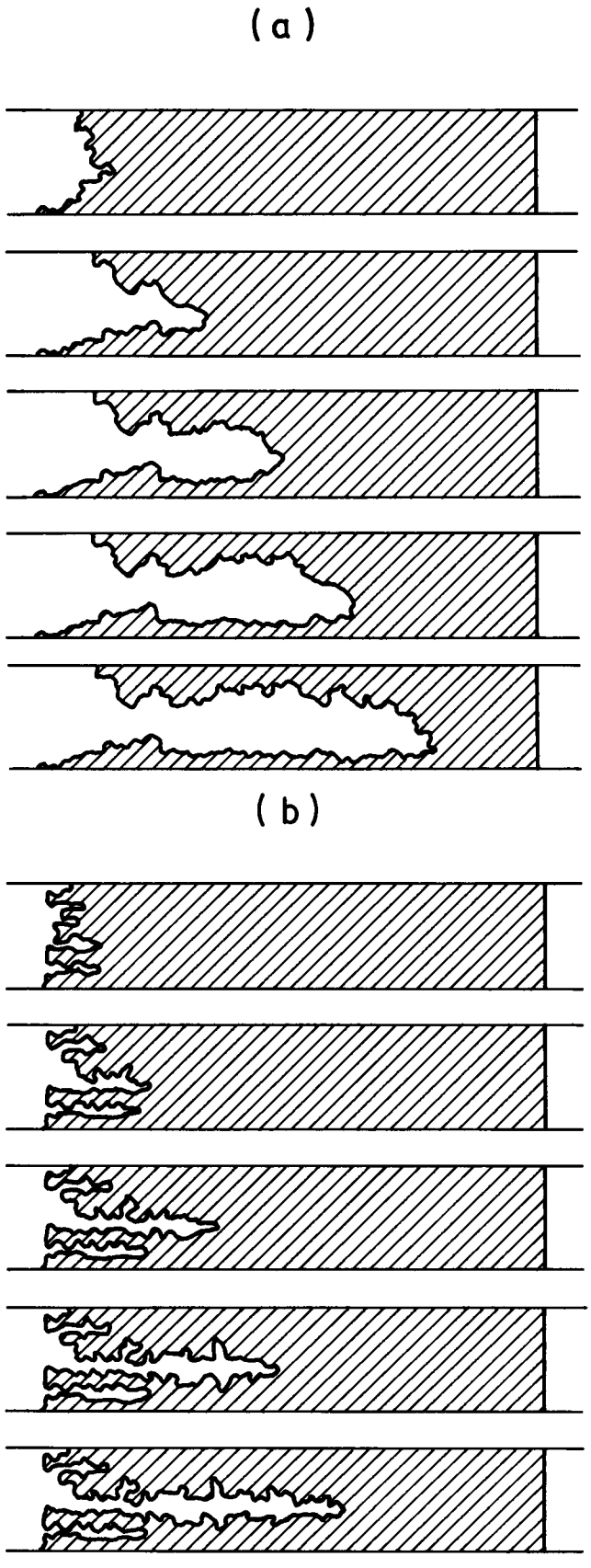

scales δ to the formula

$$L(\delta) = b\delta^{1-\bar{d}}, \tag{12}$$

where $\bar{d}$ is the fractal dimension and the constant b would be equal to the length for a one-dimensional line (Feder, 1988). Experimental lysing patterns have a fractal dimension between 1.3 and 1 (Fig. 4). Here the fractal dimension was calculated for the length scales between a few pixels (1 pixel from the MRI image ~0.2 mm) and the finger width.

From Fig. 3, *a* and *b* it is also possible to determine the dissolution velocity, i.e., the velocity of the finger growth. Although this velocity is $\sim 8 \times 10^{-3}$ lattice units (1 lattice unit ~0.2 mm) per unit time t_0 (~ 2 s) in the case of a nonzero reaction time $t_R = 500\ t_0$ (Fig. 3 *a*), it is $>11 \times 10^{-3}$ lattice units per the same unit of time in the case of the zero reaction time. The velocity of the finger growth increases with time as $v \sim t^{0.35}$ (Liang, 1986) in the "pedestrian model," which is close to the DLA result $v \sim t^{0.4}$. However, this is only true for the fingers that are not large compared with the cell width W. A similar time dependence of the velocity was found (Liang, 1986) for the growth of the mixing zone θ, which is defined as the distance along the flow direction between the tips of the largest fingers in each direction. The velocity $d\theta/dt$ increases with time for small fingers, but it becomes constant when the length of the mixing zone θ is larger than the width of the cell W. This is consistent with our results where the velocity of the finger growth is approximately constant if the fingers are long compared with the width of the clot.

In our experiments, the observed reaction time was ~15 min (Zidanšek and Blinc, 1991; Blinc et al., 1991). This is relatively small compared with the recanalization time, i.e., the time necessary for the dissolved finger to pass through the whole retracted clot which was a few hours. The diffusion transport terms are small compared with the perfusion transport. After 5 h of dissolution, the activator front boundary is spread for about $\langle r^2 \rangle^{1/2} \sim 2\ Dt < 1$ mm, which is small compared with the clot size of 30 mm. Here the diffusion constant D is estimated to be $\sim 10^{-11}$ m^2 s^{-1} (Zidanšek and Blinc, 1991).

Our random walk model thus provides one of the possible explanations for a nonplanar lysis. This could also be caused, however, by dynamic instability of the interface,

FIGURE 3 Theoretical dissolution patterns, obtained from the enzyme transport limited random walk model for different values of the reaction time t_R. The modified Liang's model without the surface tension was used (Liang, 1986) with the following values of calculation parameters: the clot width $W = 22$ lattice units, the clot length $L = 100$ lattice units, and the constant M, which is described in Appendix A, is equal to 10. (*a*) A nonzero value of the reaction time $t_R = 500t_0$ (with $t_0 \sim 2$ s) leads to wide fingers indicated. The time interval between the slices is $\Delta t = 2000t_0$. (*b*) The instant reaction approximation ($t_R = 0$) gives narrow and fast growing fingers with a fractal dimension close to the theoretical value for the diffusion limited aggregation patterns $\bar{d} \approx 1.7$ (Vicsek, 1989) only at early times, whereas the fractal dimension is decreasing at later times. The clot boundaries are here represented at equal time intervals $0.5\Delta t = 1000t_0$.

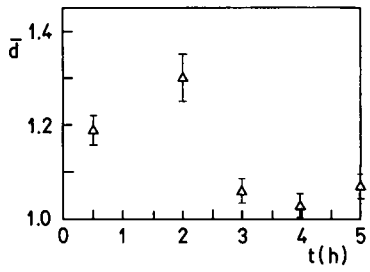

FIGURE 4 Time evolution of the fractal dimension of the observed lysing patterns (Fig. 1), obtained from the fit to Eq. 12 for the length scales between 5 pixels and the finger width.

large spatial variation of porosity in the clot, or no-slip boundary condition at the wall. We believe that large scale variation of porosity is not very likely, because fingering was also observed in clots, which previously were not retracted and glued to the glass wall but were obtained from homogeneously mixed blood (Blinc et al., 1994). Dynamic instability of the interface is not very likely because of the low Reynolds numbers for the flow through the clot (Re $< 10^{-6}$). We have also shown that the non-slip boundary condition combined with the Brinkman equation (Eq. 11) is effective only in the narrow surface region less than a micrometer from the glass-clot boundary and, thus, cannot be responsible for the fingering.

CONCLUSIONS

The finger-like drug-induced blood clot dissolution patterns observed by MRI indeed can be described by the enzyme transport-limited system of fibrinolytic chemical reactions with diffusion and perfusion terms in the reaction time approximation if the random character of clot porosity is taken into account. The fractal dimension of the experimental lysing patterns changes from 1.2 at the beginning of the experiments to a maximum of ~1.3 in the middle and then decreases toward 1 when the clot is recanalized.

Our random walk simulation shows remarkable similarities to experimental and clinical observations not only in the velocity of clot lysis but also in the dependence of the shape of the lysing patterns on the enzyme transport parameters. Bugelski and co-workers have shown by electron microscopy that lysis of coronary artery thrombi in dogs proceeds through meandering channels that eventually merge into a dominant recanalization channel, leaving substantial parts of the clot intact (Bugelski et al., 1989). Radiological studies in humans have confirmed that finding a residual thrombus after successful vessel recanalization by fibrinolysis is a rule rather than an exception (Brown et al., 1986; Gash et al., 1986; Gulba et al., 1990).

According to our in vitro MRI observations and the random walk model of thrombus dissolution, the cost for rapid recanalization is a residual nonlysed part of the thrombus. Our model also demonstrates that the peripheral parts of occlusive thrombi with a concave proximal border dissolve slowly because of their disadvantaged position with respect to the local pressure gradients and not necessarily because of low fibrinolytic susceptibility.

APPENDIX A

Random walk simulation of the fibrinolytic system

Here one first calculates for a given clot shape the pressure field inside the clot. The model clot is described as a discrete two-dimensional network of points G with width of W points and length of L points, surrounded by the boundaries B_1, B_2, and B_3. All of the boundary points are located in the middle of two lattice points. With a given solution for the pressure field, the flow velocity $\mathbf{v}_F$ at any point inside the clot is obtained from Eq. 8.

If the fluid is incompressible ($\nabla \mathbf{v}_F = 0$), the Laplace equation for the pressure field p is obtained:

$$\nabla^2 p = 0. \tag{13}$$

The pressure field p inside the clot can be expressed as a sum over a geometry-dependent Green's functions $g(\mathbf{r}, \mathbf{s})$ weighted by the boundary values $\psi(\mathbf{s})$ (Liang, 1986):

$$p(\mathbf{r}) = \sum_s g(\mathbf{r}, \mathbf{s})\psi(\mathbf{s}). \tag{14}$$

Here the boundary values $\psi(\mathbf{s})$ represent the pressure at the boundary and Green's function $g(\mathbf{r}, \mathbf{s})$ solves the Laplace equation for the points $\mathbf{r}$ inside a given region with the boundary condition that $\psi = 1$ at the boundary point $\mathbf{s}$ and 0 everywhere else (see Appendix B).

It was shown (Kadanoff, 1985) that Green's function $g(\mathbf{r}, \mathbf{s})$ for an arbitrary region can be calculated with a random walk simulation (see Appendix C).

In our simulations, the region of interest (i.e., the clot) is divided into two parts, using the analytical solution for the Green's function (Appendix B) in the first part and the random walk simulation (Appendix C) in the other. The rectangle (region I) is surrounded by the boundaries B_2 (the outflow plasma-clot boundary), B_3 (the clot-vessel boundary), and the line B_5, which is parallel to the outflow plasma-clot boundary B_2 and lies between the outflow plasma-clot boundary B_2 and the activator front boundary B_4 (Fig. 2 *b*). The remainder of the clot (region II) is made of the reaction region between the inflow plasma-clot boundary B_1 and the activator front boundary B_4, and an irregular region without enzymes between the boundaries B_1, B_3, B_4, and B_5 (Fig. 2*b*).

The boundary conditions from Appendix C are modified in such a way that the random walkers are released from the boundary B_5 instead of the outflow blood clot boundary B_2. If a given random walker hits the boundary B_5, it enters the region I (the rectangle). Because the probability that it will return to the region II at the point $\mathbf{s}$ is given by Green's function for the half plane, which is calculated analytically (Appendix B), the random walker is returned to the region II at point $\mathbf{s}$ with the probability

$$P(\mathbf{s}) = g_v(\mathbf{r}, \mathbf{s}), \tag{15}$$

where g_V is Green's function for the half plane. If the expected returning point is outside region I, the corresponding half plane is bent so many times that the returning point comes inside the rectangle according to the reflexive boundary condition at the clot-vessel boundary B_3.

The numerical simulation begins with a rectangular shape of the clot, where initially the boundaries B_1 and B_4 are equal and planar. The activator front boundary B_4 is moved according to the Darcy's law (Eq. 8), where the pressure p at a given point $\mathbf{r}$ is proportional to the probability $P(\mathbf{r})$ that this point is visited by a single random walker (Appendix C). The motion of the activator front boundary B_4 is obtained, therefore, by counting the number

of random walkers $N(\mathbf{r})$ traveling through every point $\mathbf{r}$ of the activator front boundary B_4 in the direction to the reaction region (Fig. 2 *b*). When this number is larger then a given constant M or smaller than $-M$, then both lattice points, which are the closest to the activator front boundary point $\mathbf{r}$, are assigned to the reaction region or to the nonreaction region, respectively, and the activator front boundary B_4 is moved accordingly. At the same time, the inflow blood-clot boundary B_1 is moved according to Eq. 10, and the boundary B_5 between the regions I and II is moved for one lattice point to the right if it crosses the new activator front boundary B_4. Here the number M stands for the pressure difference between the observed pair of lattice points, which is required to move the boundary for one lattice point according to the Darcy's law (Eq. 8), and the pressure is measured in units of probability (Kadanoff, 1985).

This procedure is repeated until the activator front boundary B_4 reaches the outflow blood-clot boundary B_2. At that time, the boundary B_5 becomes equal to the outflow blood-clot boundary B_2 and the random walk simulation is performed in region II only. When the inflow blood-clot boundary B_1 reaches the outflow blood-clot boundary B_2 also, the clot is recanalized and the calculation is finished. The time evolution of the inflow blood-clot boundary $B_1(t)$ represents the fibrinolytic patterns.

APPENDIX B

Properties of the lattice Green's function

The boundary condition for the lattice Green's function in the points $\mathbf{r}$ can be written in terms of the lattice Dirac function

$$g(\mathbf{r}, \mathbf{s}) = \delta(\mathbf{r}, \mathbf{s}), \tag{16}$$

where the function $\delta(\mathbf{r}, \mathbf{s}) = 0$ unless $\mathbf{r} = \mathbf{s}$ when $\delta(\mathbf{r}, \mathbf{r}) = 1$. Green's function $g(\mathbf{r}, \mathbf{s})$ obeys the lattice version of the Laplace equation

$$\nabla^2 g(\mathbf{r}, \mathbf{s}) = 0 \tag{17}$$

for the points $\mathbf{r}$ inside the clot where the operator ∇ stands for a derivative with respect to $\mathbf{r}$. The discrete lattice Laplacian ∇^2 is defined here as (Kadanoff, 1985):

$$\begin{aligned}\nabla^2 f(x, y) = 4f(x, y) - f(x + 1, y) - f(x - 1, y) \\ - f(x, y + 1) - f(x, y - 1),\end{aligned} \tag{18}$$

where $f(x, y)$ is any function defined on the lattice points x, y inside the region of interest (i.e., inside the clot), where the integers x and y count the lattice points.

Green's function g_d for an infinite d-dimensional regular lattice can be written as

$$g_d(\mathbf{x}, \mathbf{y}) = \lim_{N\to\infty} \frac{1}{N} \sum_{\mathbf{k}} \frac{a^2}{2\sum_{j=1}^{d}(1 - \cos(k_j a))} \exp(i\mathbf{k} \cdot (\mathbf{x} - \mathbf{y})), \tag{19}$$

where a is the distance between the neighboring lattice points and the sum is taken over all of the reciprocal lattice vectors $\mathbf{k}$. Green's function for a half plane, which includes all of the points with the second (y) coordinate larger than H, can be obtained as (Kadanoff, 1985):

$$g_v(\mathbf{x}, \mathbf{y}) = g(\mathbf{x} - \mathbf{y}) - g(x_1 - y_1, x_2 + y_2 - 2H), \tag{20}$$

where

$$g(\mathbf{x} - \mathbf{y}) = g_2(\mathbf{x}, \mathbf{y}), \tag{21}$$

and $\mathbf{x} = (x_1, x_2)$ and $\mathbf{y} = (y_1, y_2)$. The function $g(\mathbf{x})$ can be calculated by replacing the sum with an integral:

$$g(\mathbf{x}) = \int_{-\pi}^{\pi} \frac{dk_x}{2\pi} \int_{-\pi}^{\pi} \frac{dk_y}{2\pi} \frac{1}{4 - 2\cos k_x - 2\cos k_y} \exp(i\mathbf{k} \cdot \mathbf{x}). \tag{22}$$

This integral diverges, but it is possible to calculate the difference $g(\mathbf{x}) - g(0)$ analytically. For large $\mathbf{x}$ the asymptotic result is

$$g(\mathbf{x}) - g(0) \sim \frac{1}{2\pi}(\log|\mathbf{x}| + \log(2\sqrt{2}) + \gamma), \tag{23}$$

where $\gamma \sim 0.5772166$ is the Euler constant.

APPENDIX C

Random walk solution of the Laplace equation

In the case of our blood clot model, the lattice Green's function $g(\mathbf{r}, \mathbf{s})$ is proportional to the probability $P(\mathbf{r})$ that the point $\mathbf{r}$ inside the clot is visited by the random walker, which is released from the point $\mathbf{s}$ on the outflow plasma-clot boundary B_2 and is annihilated when it hits the inflow plasma-clot boundary B_1 (see Fig. 2 *b*). At a given time step, the random walker travels to any of its four neighboring points with the probability 0.25. If it hits the clot-vessel boundary B_3, it is reflected back into the clot because there can bo no flow through the vessel wall. When the random walker is annihilated, the next random walker is released from point $\mathbf{s}$. The probability $P(\mathbf{r})$ can be calculated as

$$P(\mathbf{r}) = \frac{N(\mathbf{r})}{\mathrm{N}}, \tag{24}$$

where N is the number of released random walkers and $N(\mathbf{r})$ counts the number of visits for a given point $\mathbf{r}$. The probability $P(\mathbf{r})$ obeys the boundary condition of Green's function (Eq. 16): because every random walker is released from the point $\mathbf{s}$, $P(\mathbf{s}) = 1$ and $P = 0$ for all other boundary points because the visit of any boundary point terminates a given random walk. The lattice Laplace equation (Eq. 17) is also satisfied because every lattice point is visited only by the random walks from the neighboring points. Because the probability that a given random walker at the neighboring lattice site chooses the right direction is 0.25, the probability $P(\mathbf{r})$ is given as

$$P(\mathbf{r}) = \frac{1}{4} \sum_{\langle\,\rangle} P(\mathbf{r}'), \tag{25}$$

where the sum $\sum_{\langle\,\rangle}$ is taken over all of the neighboring sites. Using the definition of the lattice Laplace operator (Eq. 18), we have

$$\nabla^2 P(\mathbf{r}) = 4P(\mathbf{r}) - \sum_{\langle\,\rangle} P(\mathbf{r}') = 0. \tag{26}$$

The probability $P(\mathbf{r})$ thus obeys the boundary condition (Eq. 16) and the Laplace equation inside the clot (Eq. 17) and, therefore, is equal to Green's function $g(\mathbf{r}, \mathbf{s})$. If $\mathbf{r}$ and $\mathbf{s}$ are the boundary points between the two lattice points (Fig. 2 *b*), Green's function $g(\mathbf{r}, \mathbf{s})$ is equal to the probability that a random walker that enters the region of interest through boundary point $\mathbf{s}$ will leave through boundary point $\mathbf{r}$.

REFERENCES

AIMS Trial Study Group. 1990. Long term effects of intravenous anistreplase in acute myocardial infarction: final report on the AIMS study. *Lancet.* 335:427–431.

Blinc, A., G. Planinšič, D. Keber, O. Jarh, G. Lahajnar, A. Zidanšek, and F. Demsar. 1991. Dependence of blood clot lysis on the mode of transport of urokinase into the clot: a magnetic resonance imaging study in vitro. *Thromb. Haemost.* 65:549–552.

Blinc, A., D. Keber, G. Lahajnar, M. Stegnar, A. Zidanšek, and F. Demsar. 1993. Lysing patterns of retracted blood clots with diffusion or bulk flow transport of plasma with urokinase into clots: a magnetic resonance imaging study in vitro. *Thromb. Haemost.* 68:667–671.

Blinc, A., S. D. Kennedy, R. G. Bryant, V. J. Marder, and C. W. Francis. 1994. Flow through clots determine the rate and pattern of fibrinolysis. *Thromb. Haemost.* 71:230–235.

Brown, B. G., C. A. Gallery, R. S. Badger, J. W. Kennedy, D. Mathey, E. L. Bolson, and H. T. Dodge. 1986. Incomplete lysis of thrombus in the moderate underlying atherosclerotic lesion during intracoronary infusion of streptokinase for acute myocardial infarction: quantitative angiographic observations. *Circulation.* 73:653–661.

Bugelski, P. J., G. A. Kopia, L. Kopaciewicz, A. S. Cadogan, and D. G. Morgan. 1989. Ultrastructural analysis of thrombolysis by streptokinase and tissue type plasminogen activator of experimental coronary arterial thrombosis. *Fibrinolysis.* 3:137–145.

Carr, M. E., and C. L. Hardin. 1987. Fibrin has larger pores when formed in the presence of erythrocytes. *Am. J. Physiol.* 253:H1069–H1073.

Daccord, G., and R. Lenormand. 1987. Fractal patterns from chemical dissolution. *Nature.* 325:41–43.

Diamond, S. L., and S. Anand. 1993. Inner clot diffusion and permeation during fibrinolysis. *Biophys. J.* 65:2622–2643.

Feder, J. 1988. Fractals. Plenum Press, New York. 8 pp.

Gash, A. K., J. F. Spann, S. Sherry, A. D. Belber, B. A. Carabello, M. T. McDonough, R. H. Mann, W. D. McCann, J. H. Gault, R. D. Gentzler, and R. L. Kent. 1986. Factors influencing reocclusion after coronary thrombolysis for acute myocardial infarction. *Am. J. Cardiol.* 57: 175–177.

GISSI (Gruppo Italiano per lo Studio della Streptochinasi nell'Infarcto Miocardico). 1987. Long term effects of intravenous thrombolysis in acute myocardial infarction: final report of the GISSI study. *Lancet.* 2:871–874.

Gulba, D. C., C. Bode, J. Topp, H. W. Hopp, M. Westhoff-Bleck, W. Rafflenbleul, and P. R. Lichtlen. 1990. Die Haufigkeit von Residualthromben nach erfolgereicher Thrombolysetherapie bei akutem Herzinfarkt und ihre Bedeutung fur die Rate fruher Reokklusionen. *Z. Kardiol.* 79:279–285.

ISIS-2 (Second International Study of Infarct Survival) Collaborative Group. 1988. Randomized trial of intravenous streptokinase, oral aspirin, both or neither among 17187 cases of suspected acute myocardial infarction: ISIS-2. *Lancet.* 2:349–360.

Kadanoff, L. 1985. Simulating hydrodynamics: a pedestrian model. *J. Stat. Phys.* 39:267–283.

Liang, S. 1986. Random-walk simulations of flow in Hele-Shaw cells. *Phys. Rev. A.* 33:2663–2674.

Martys, N., D. P. Bentz, and E. J. Garboczi. 1994. Computer simulation study of the effective viscosity in Brinkman's equation. *Phys. Fluids.* 6:1434–1439.

Senf, L. 1979. In-vitro-Untersuchungen und Modellrechnungen zur Kinetik der Fibrinolyse durch Streptokinase. *Folia Haematol.* 106:899–907.

Stampfer, M. J., S. Z. Goldhaber, S. Yusuf, R. Peto, and C. H. Hennekens. 1982. Effect of intravenous streptokinase on acute myocardial infarction: pooled results from randomized trials. *N. Engl. J. Med.* 307:1180–1182.

Yusuf, S., R. Collins, R. Peto, M. J. Furberg, M. J., Stampfer, S. Z. Goldhaber, and C. H. Hennekens. 1985. Intravenous and intracoronary fibrinolytic therapy in acute myocardial infarction: overview of results on mortality, reinfarction and side effects from 33 randomized trials. *Eur. Heart J.* 6:556–585.

Vicsek, T. 1989. Fractal Growth Phenomena. World Scientific, Singapore. 138 pp.

Weinstein, M. J., and R. F. Doolittle. 1972. Differential specificities of thrombin, plasmin and trypsin with regard to synthetic and natural substrates and inhibitors. *Biochim. Biophys. Acta.* 258:577–90.

Zidanšek, A., and A. Blinc. 1991. The influence of transport parameters and enzyme kinetics of the fibrinolytic system on thrombolysis: mathematical modelling of two idealized cases. *Thromb. Haemost.* 65: 553–559.

Zidanšek, A., A. Blinc, G. Lahajnar, D. Keber, and R. Blinc. 1993. Lysing patterns of blood clots: a nuclear magnetic resonance imaging study in vitro and mathematical modelling of the lysing pattern kinetics. *J. Mol. Struct.* 294:283–286.